Electrically tunable helicity of cholesteric heliconical superstructure [Invited]

Conglong Yuan (袁丛龙)[1], Wenbin Huang (黄文彬)[1,2], Xiaoqian Wang (王骁乾)[1], Dong Shen (沈 冬)[1], and Zhigang Zheng (郑致刚)[1,3,*]

[1]*Department of Physics, East China University of Science and Technology, Shanghai 200237, China*
[2]*School of Optoelectronic Science and Engineering & Collaborative Innovation Center of Suzhou Nano Science and Technology, Soochow University, Suzhou 215006, China*
[3]*Advanced Materials and Liquid Crystal Institute and Chemical Physics Interdisciplinary Program, Kent State University, Kent, Ohio 44242, USA*
**Corresponding author: zgzheng@ecust.edu.cn*

Received May 20, 2020; accepted June 23, 2020; posted online July 16, 2020

The dynamic manipulation of the helicity in a cholesteric helical superstructure could enable precise control over its physical and chemical properties, thus opening numerous possibilities for exploring multifunctional devices. When cholesteric material satisfies the sufficiently small bending elastic effect, an electrically induced deformation named the cholesteric heliconical superstructure is formed. Through theoretical and numerical analysis, we systematically studied the tunable helicity of the heliconical superstructure, including the evolution of the corresponding oblique angle and pitch length. To further confirm the optical properties, Berreman's 4×4 matrix method was employed to numerically analyze the corresponding structure reflection under the dual stimuli of chirality and electric field.

Keywords: cholesteric liquid crystal; heliconical superstructure; tunable reflection band; electro-optical materials.
doi: 10.3788/COL202018.080005.

The ability of controlling and manipulating the rearrangement of molecules through external stimuli to obtain tunable and reversible structural characteristics is a major driving force towards the development of multifunctional devices. The cholesteric liquid crystal (CLC) or chiral nematic liquid crystal (LC) with self-organized helical superstructure and typical stimulus-response characteristics has undoubtedly served as a model system for better understanding orientation-related supramolecular dynamic helical structures and exploring their potential in technological applications[1–6]. Under the induction of chiral interaction, LC molecules in the cholesteric phase rotate around a helical axis and remain perpendicular, forming a so-called right-angle helicoid. The characteristic pitch length and specific handedness of the CLC architectures can be readily modulated through external stimuli such as temperature, light, and electric field[7–10]. The pitch, representing periodicity, is the distance along the helical axis when LC molecules complete 2π rotation, while the handedness indicates the rotation direction, e.g., left-handedness or right-handedness. The planar aligned helical architecture endows CLC with a significant selective reflection band or photonics bandgap[11]. It separates the light propagating along the helical axis into right-handed and left-handed circularly polarized components. One component of the same handedness as the cholesteric is reflected, while the other component is transmitted. The central reflection wavelength λ_c is determined by the average refractive index $\bar{n}$ and the helical pitch P of the CLC system, expressed as $\lambda_c = \bar{n}P$ in the case of normal incidence. When the wavelength of incident light is on the order of pitch length, it exhibits typical structure color[12,13]. Tremendous explorations and efficient endeavors in recent decades have been devoted to dynamically manipulating the reflection band shift, thus achieving diverse applications ranging from thermosensitive sensors, smart windows, light-directed diffraction optical elements, tunable mirrorless lasing, and tunable color filters[14–21]. Among numerous external stimuli, the electric field undoubtedly has absolute priority, due to its superior advantages of stability, and instantaneous, precise, and programmable controllability. However, when the applied electric field is parallel to the helical axis, only a limited range of pitch tuning can be obtained in the right-angle helicoid without reorienting the helical axis[22,23] due to complicated competition between electric-field-induced LC rearrangement from the dielectric anisotropy and the twist torque from chirality.

As early as 50 years ago, Meyer and de Gennes[24,25] predicted that if the bend elastic constant K_3 is much smaller than twist elastic constant K_2 of the CLC system, there would be a unique external-field-induced deformation state, named the CLC heliconical state, also known as an oblique helicoid, in which the helical LC director is tilted with an oblique angle to the helical axis. One of the most critical advantages of such a CLC heliconical state is that it exhibits a wide range of tunable selective reflection band, because the applied electric field does not disturb the helical axis but provides a wide range of dynamic and reversible tuning of oblique angles and pitch

lengths. However, it is commonly hard to explore such a unique superstructure experimentally due to the lack of materials with the necessary elastic effect coupling[26]. For example, the well-known rod-like LC 5CB has $K_1 = 6.4\,\mathrm{pN}$, $K_2 = 3.0\,\mathrm{pN}$, and $K_3 = 10.0\,\mathrm{pN}$ at room temperature[27]. Fortunately, recent developments concerning the twist–bend nematic (N_{tb}) phase have found that bend-shaped LC dimers or trimers furnish sufficiently smaller K_3 than K_2. For instance, an LC dimer CB7CB, which consists of two rod-like cyanobiphenyl moieties directly linked by a flexible alkyl chain, has its $K_1 \approx 5.7\,\mathrm{pN}$, $K_2 \approx 2.6\,\mathrm{pN}$, and $K_3 \approx 0.3\,\mathrm{pN}$ at 103°C[28]. K_3 drops further as the materials cooled[29]. The CLC heliconical superstructure formed by a mixture of CB7CB and chiral dopant S811 was observed in a polarizing optical microscopy study and Ramn–Nath diffraction[30]; however, it only exists in a very limited high temperature range between 103°C and 116°C. Adding a certain amount of nematic LC to judiciously optimize the cholesteric composition can not only maintain the necessary elastic effect coupling, but also greatly extend the operating temperature range to room temperature. Thus, a wide range of modulated selective reflection bands spanning from UV to near IR from the heliconical superstructure have been established[15,31–33]. Alternatively, the structure can also be established and driven by a magnetic field[34]. In our recent work[35], we have further expanded the controlling dimension of the CLC helical superstructure. Under a dual stimulation of electric field and light irradiation, a reversible and dynamic transition between the helicoidal state and heliconical state and their inverse helices together with a modulation of helical pitch length and oblique angle were achieved.

In this Letter, we demonstrated the theoretical framework of the electrically induced CLC heliconical superstructure and employed numerical simulations to quantitatively evaluate the importance of the bend and twist elastic effects on the formation and tunability of the superstructure, as well as the evolution of pitch length and oblique angle. To further confirm the optical properties of the heliconical superstructure, we utilized the Berreman's 4×4 matrix method to numerically analyze the corresponding selective reflection characteristics, including the circular polarization selectivity, reflective intensity, and the reflection band shifting under the dual stimuli of applied electric fields and system chirality.

The electric-field-induced LC director arrangement can be described by using the Oseen–Frank free energy function. The elastic energy density for the CLC helical superstructure is written as

$$f = \frac{1}{2}[\,K_1(\nabla \cdot \hat{n})^2 + K_2(\hat{n} \cdot \nabla \times \hat{n} - q_0)^2 + K_3(\hat{n} \times \nabla \times \hat{n})^2 - \Delta\epsilon\epsilon_0(\hat{n} \cdot \vec{E})^2], \tag{1}$$

where K_1, K_2, and K_3 are the splay, twist, and bend elastic constant, respectively; $\hat{n}$ is a unit vector denoting the LC director; $q_0 = 2\pi/P_0$, representing the system chirality

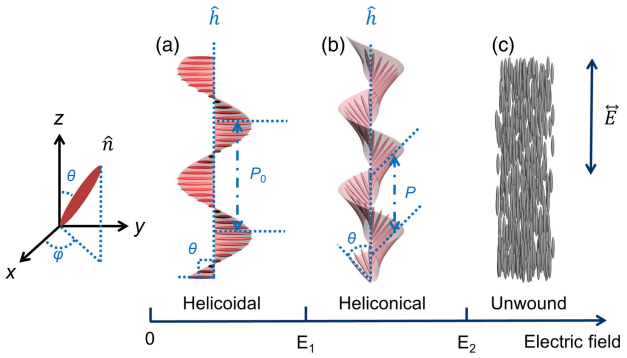

Fig. 1. Schematic illustration of LC director configurations in cholesteric (a) helicoidal, (b) heliconical, and (c) unwound states under increased applied electric fields.

determined by the chemical composition; P_0 is the initial pitch length when there is no electric field; $\Delta\epsilon = \epsilon_{\parallel} - \epsilon_{\perp}$, is the dielectric anisotropy, representing the difference between the dielectric constant of the LC director along the long axis and the short axis; ϵ_0 is the permittivity of vacuum; $\vec{E}$ is the external electric field. Generally, the electric-field correlation of the CLC structure is the perturbation of the helix at low fields, followed by complete unwinding at a certain threshold field. As shown in Fig. 1, we consider that there is a longitudinal electric field $\vec{E} = (0,\ 0,\ E)$ applied to CLC with positive dielectric anisotropy, and we assume that the boundary conditions will keep the axis of the helix $\hat{h}$ (z axis) parallel to the field. The LC director is

$$\hat{n} = (\cos\phi\sin\theta,\quad \sin\phi\sin\theta,\quad \cos\theta), \tag{2}$$

defined by a polar angle θ and an azimuth angle ϕ. By minimizing the free energy [Eq. (1)], we got the following three stacked configurations of LC molecules: helicoidal, heliconical, and unwound state, as indicated in Figs. 1(a), 1(b), and 1(c), respectively.

In the absence of an external electric field, the chirality from intermolecular interaction will guide the LC molecules to self-organize into a helicoidal superstructure, where the LC director twists at a right angle around the helical axis $\hat{h}$, as shown in Fig. 1(a). Then, LC director $\hat{n}$ in the helicoidal state is given by $\hat{n} = (\cos\phi(z),\ \sin\phi(z),\ 0)$. Considering a left-handedness helix, then it can be further expressed as

$$\hat{n} = \left(\cos\left(-\tfrac{2\pi}{P_0}z\right),\quad \sin\left(-\tfrac{2\pi}{P_0}z\right),\quad 0\right). \tag{3}$$

The azimuth angle $\phi(z) = -2\pi z/P_0$, is determined by the position of the LC on the z axis, and the negative sign indicates left-handedness. When an electric field parallel to $\hat{h}$ is applied, the distortion in the CLC system involves both bending and twisting, which depends on the relative magnitudes of the twist elastic constant K_2 and bend elastic constant K_3. If $K_3 > K_2$, there is no distortion until the electric field reaches a threshold value E_2, where

the helix is completely unwound into a homeotropic alignment, as shown in Fig. 1(c), in which the LC director everywhere is parallel to the field, i.e.,

$$\hat{n} = (0, \quad 0, \quad 1). \tag{4}$$

For $K_3 < K_2$, it can reach a regime under the action of the external electric field, where there is a delicate equilibrium between bending and twisting elastic effects and a competitive coupling between the dielectric torque and the twist torque of the CLC system, resulting in the heliconical state, in which the helix remains unchanged without any distortion or re-orientation, and the director $\hat{n}$ rotates around the helix with an oblique angle θ $(0 < \theta < \pi/2)$, as shown in Fig. 1(b). Then, the director $\hat{n}$ in the heliconical state can be written as

$$\hat{n} = \left(\cos\left(-\tfrac{2\pi}{P}z\right)\sin\theta, \quad \sin\left(-\tfrac{2\pi}{P}z\right)\sin\theta, \quad \cos\theta\right). \tag{5}$$

The electric-field-induced CLC heliconical superstructure exists between the helicoidal superstructure and the unwound state with the corresponding applied electric field being located between the lower induction threshold E_1 and the upper unwinding threshold E_2, which can be calculated by the following equations:

$$E_2 = \frac{2\pi}{P_0}\frac{K_2}{\sqrt{\Delta\epsilon\epsilon_0 K_3}}, \tag{6}$$

$$E_1 \approx E_2\frac{\eta[2+\sqrt{2(1-\eta)}]}{1+\eta}, \tag{7}$$

where $\eta = K_3/K_2$ is the ratio of the bend and the twist elastic constants, denoting the elastic effect coupling. Equation (7) is an approximation in the case of a small η. One of the critical advantages of the CLC heliconical state is the peculiar tunable performance. Without deforming the helical axis, it can rearrange the LC director along itself and then reduce the P and θ under the increasing of the electric field, which can be calculated by

$$P = \frac{2\pi}{E}\sqrt{\frac{K_3}{\epsilon_0\Delta\epsilon}}, \tag{8}$$

$$\sin^2\theta = \frac{\eta}{1-\eta}\left(\frac{E_2}{E}-1\right). \tag{9}$$

The CLC heliconical state demonstrated here is distant from the electric-induced layer undulation of the ordinary CLC, which usually exhibits fingerprint texture[36], or the similar arrangement of the LC director in the chiral smectic C phase[37] and the N_{tb} phase[38]. The latter formed by achiral molecules allows the coexistence of left-handed and right-handed domains and shows only a very short pitch length of about 10 nm. While in semectic C phase, the θ is a certain molecular tilt angle fixed in semectic layers, and the structure depends on the sense of molecular orientation and materials density.

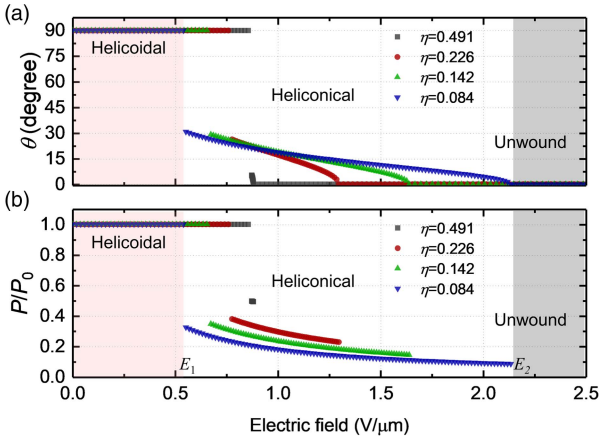

Fig. 2. Electrical tuning performance of the (a) oblique angle θ and (b) pitch length P in helicoidal, heliconical, and unwound states with various η value.

Then, we employed numerical calculations to quantitatively describe the phase diagram of the CLC heliconical superstructure and the importance of the η value for the θ and P changes under the application of an electric field. As shown in Fig. 2, with the gradual increase of the electric field, we obtained the evolution of P and θ in the helicoidal, heliconical, and unwound states. Without the applied electric field, the LC director arranges into the helicoid with an initial pitch length P_0 and an oblique angle at 90°. When the electric field is below the first threshold E_1, even if the electric field increases, there is no obvious deformation in the helicoid state, thus the corresponding P and θ remain almost unchanged (i.e., $P/P_0 \approx 1$, $\theta \approx 90°$). Taking $\eta = 0.083$ as an example, as the electric field increases beyond the threshold E_1, the helicoid state transforms to the heliconical state. During the phase transition, such electric-field-induced deformation first generates an overall tilt and contraction, which is manifested by its oblique angle suddenly jumping from 90° to about 30° and the pitch shrinking to about 0.3 times the initial pitch $(P/P_0 \approx 0.3)$. Subsequently, both P and θ continue to decrease with the increase of the electric field until it exceeds the threshold E_2, and then the P and θ gradually approach zero and infinity, respectively. Finally, all LC molecules are completely unwound and parallel to the direction of the electric field. It is worth noting that the tunable range of the oblique angle and relative pitch length depends only on the η value, irrespective of other parameters. The smaller the η, the wider the electric-field tunable range of the heliconical structure becomes.

The initial chirality (or initial pitch length P_0) of the system is also of great significance during the formation and tuning of the oblique angle and pitch length in the heliconical superstructure. In addition, the advanced light-responsive CLC systems manipulating their helical characteristics are based on the mechanism that light irradiation changes the initial system chirality[39,40]. Therefore, the

discussion here can also help with understanding the optical and electrical dual-response characteristics of the heliconical state when photosensitive chiral dopants are mixed in the CLC system. Defined as $q_0 = 2\pi/P_0$, chirality denotes the system chiral strength, determined by the concentration and helical twisting power of the chiral dopants. In order to better express the switching and tuning performances of the CLC system, we assume that the material has a small η value ($\eta = 0.083$). With the gradual enhancement of the chirality q_0, Fig. 3 illustrates the evolution of the transformation thresholds E_1 and E_2 for the appearance and disappearance of the heliconical state [Fig. 3(a)] and the development of the oblique angle θ [Fig. 3(b)] and pitch length P [Fig. 3(c)] in the helicoidal, heliconical, and unwound states under several certain electric-field values.

The stronger the chirality of the system, the corresponding two threshold values both show a linear increasing trend, where the slopes are related to the elastic effect coupling. In the case of weak chirality, the dielectric torque dominates the orientation of LCs, and the system is more likely to unwind under the applied electric field. Therefore, the heliconical state can only exist within a limited electric-field range. In contrast, attributed to the comparable competition between elastic toque and dielectric torque under high chirality, the system establishes better stability and is difficult to be untwisted, so the electric-field range where the heliconical superstructure can exist is extended. Then, we assume that an electric field $E = 0.58\,\mathrm{V/\mu m}$ acts on the CLC heliconical superstructure by gradually reducing the chirality to illustrate the evolution of oblique angle θ and pitch length P [Figs. 3(b) and 3(c)]. When the chirality is large enough, the CLC exhibits a common helicoidal state with $\theta = 90°$ and $P = 2\pi/q_0$, respectively. With the gradual decrease in chirality, the helicoidal state transforms into the heliconical state accompanied by an abrupt change in P and θ. Under a specific electric field, the weaker the chirality of system, the smaller the corresponding θ because the structure is easier to drive. However, once the electric field is fixed to a certain value, the pitch length will also be determined. In other words, the initial pitch length P_0 does not affect the P under any specific electric field. Eventually, when the chirality is weak enough, the CLC material will be completely untwisted so that the oblique angle and pitch length become zero and infinity, respectively.

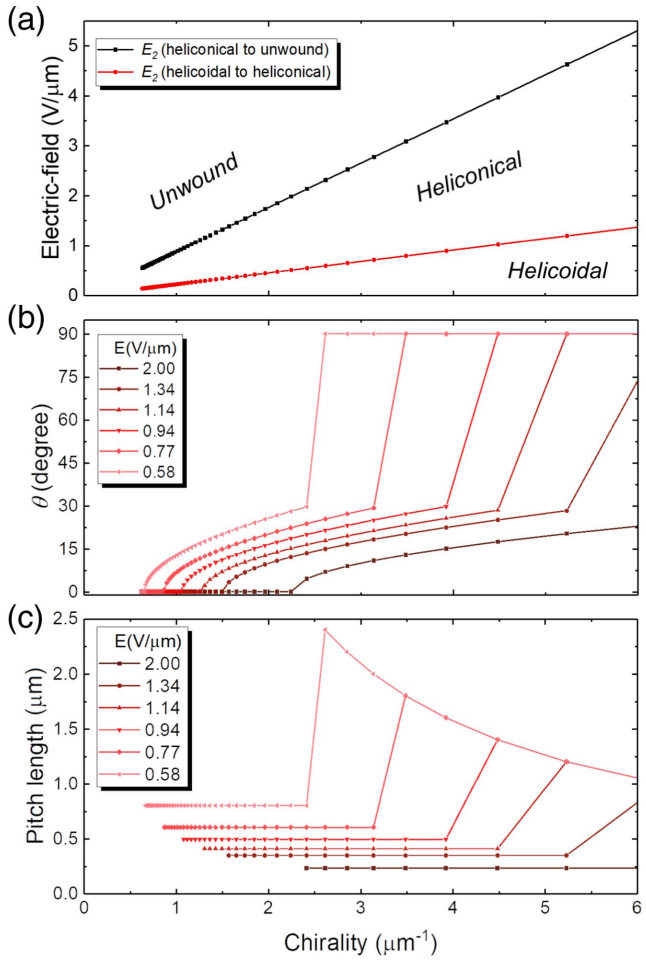

Fig. 3. Electrical tuning performance of the (a) transformation threshold, (b) oblique angle, and (c) pitch length in the heliconical superstructure on the effects of chirality changes.

Such delicate field-dependent pitch and oblique angle tunability endows the heliconical superstructure with a wide range of the periodicity and effective refractive index modulation in the spiral direction, thereby enabling selective control over the reflection band or the photonic band gap. To further evaluate the optical properties of the heliconical superstructure, we utilize Berreman's 4×4 matrix method to numerically analyze the selective reflection properties, including the circular polarization selectivity of the structural reflection band, the reflective intensity, and the reflection band shifting under different electric fields. For hierarchical optical media, its precise transmission and reflection spectral properties can be directly calculated by Berreman's 4×4 matrix method[41,42].

Consider a CLC system with the following parameters: chirality $q_0 = 2.42\,\mu\mathrm{m}^{-1}$, with left-handed helix; necessary elastic effect coupling $\eta = 0.083$; birefringence index $n_e = 1.555$, $n_o = 1.721$, ignoring the refractive index dispersion; and dielectric anisotropy $\Delta\epsilon = \epsilon_{\parallel} - \epsilon_{\perp} = 11.9 - 5.9 = 6.0$ is sandwiched in a 35 μm LC cell with a homogeneous alignment. In the situation of ideal circularly polarized light normal incidence, the corresponding structure reflection spectra from the heliconical state under some certain electric fields are shown in Fig. 4. The heliconical superstructure also exhibits the same selectivity of the Bragg reflection band to circular polarization like the helicoidal structure, e.g., the reflection only appears when the polarization state of the incident light is consistent with the helical handedness. Therefore, right-handed circularly polarized light (R-CP) will pass through the helical structure (blue line in Fig. 4). While for the case of left-handed circularly polarized light (L-CP) incidence, as the electric field gradually increases from 0.58 to 1.66 V/μm, the reflection bands exhibit a continuous and reversible shift from 1242 nm to 434 nm (because the pitch length is inversely proportional to the electric field),

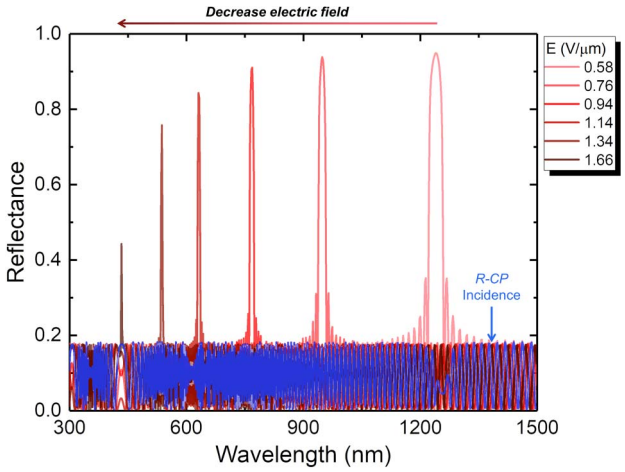

Fig. 4. Simulated selective reflection spectra from the left-handed heliconical superstructure with various electric fields in the cases of R-CP and L-CP normal incidence.

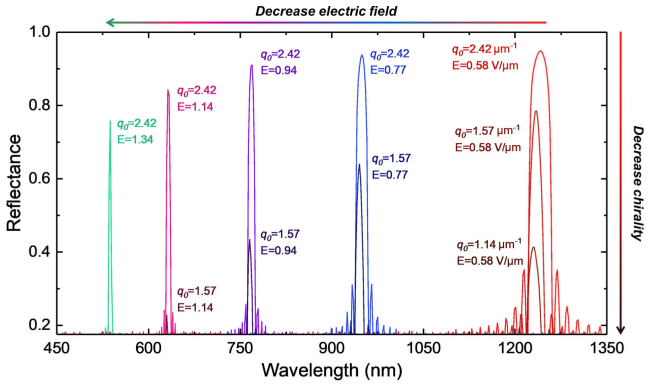

Fig. 5. Calculated reflection spectra from the heliconical superstructure with the changes of electric field and initial chirality.

accompanied by a reduced bandwidth and reflectance (since a decrease in oblique angle results in a corresponding reduction of effective birefringence). The calculation results further confirm the wide range of the electrically tunable reflection from heliconical superstructure, which is almost forbidden in the common helicoidal structure. The background interference fringes in Fig. 4 are attributed to the calculation algorithm, considering the mutual interference between the cholesteric layers.

We also simulated the effect of initial chirality change on the corresponding reflection band while maintaining the external electric field. Taking $E = 0.58\,\mathrm{V/\mu m}$ as an example, the heliconical superstructure exhibits a reflection band at 1240 nm. Gradually reducing the initial chirality of the system from 2.42 to $1.14\,\mu\mathrm{m}^{-1}$ results in a significant reduction in the reflection intensity, but with only a small spectral blue shift. A further reduction in chirality will lead to unwinding of the system, thereby completely losing the reflection. The modulation of chirality breaks the original equilibrium between the dielectric torque and the twist torque, giving rise to the prominent changes on both the arrangement transformation of the helix and the reflection performance. According to the calculation results of Figs. 3(b) and 3(c), once the electric-field value is determined, the actual pitch length is also determined. Although the decrease in initial chirality can simultaneously reduce the oblique angle, it does not shorten the pitch length. Therefore, there is no significant movement of the reflection band. On the other hand, the reduction of the oblique angle leads to a degradation of the effective refractive index modulation of the helical structure, thereby rapidly reducing the reflection intensity along with a slight spectral blue shift. The calculation in Fig. 5 also indicates that the central wavelength and the reflection intensity of the structure reflection band from heliconical state are dominated by the strength of the electric field and the system chirality, respectively. It means that the reversible switching between the existence and disappearance of the heliconical state, and the modulation of the position and intensity of the corresponding reflection band, can be accurately manipulated with a digital point-by-point or line-by-line "chirality electric field" matrix scanning.

In conclusion, we have systematically described the phase transition in a cholesteric system in the presence of a longitudinal external field parallel to the helical axis. The unique heliconical superstructure appears between the right-angle helicoidal state and unwinding state under the external field in the CLC system equipped with the necessary elastic effect of $K_3 < K_2$. Both the oblique angle and the pitch length in the heliconical superstructure decrease as the electric field decreases, thus generating a wide range of tunable selective structure reflection bands. Moreover, our calculations show that the phase behavior and helical properties can be drastically manipulated by changing the chirality. This work is useful to further understand the characteristics of the CLC heliconical superstructures and the twisting and bending distortion in the chiral system, thereby providing some new insights for further exploring scientific research and developing related multifunctional devices.

This work was supported by the National Natural Science Foundation of China (Nos. 61822504 and 51873060), the Shanghai Rising Star Program (No. 17QA1401100), and the Fundamental Research Funds for the Central Universities (No. JKM012016032).

References

1. Z. G. Zheng, Y. Li, H. K. Bisoyi, L. Wang, T. J. Bunning, and Q. Li, Nature **531**, 352 (2016).
2. Y. K. Kim, X. Wang, P. Mondkar, E. Bukusoglu, and N. L. Abbott, Nature **557**, 539 (2018).
3. N. Y. Ha, Y. Ohtsuka, S. M. Jeong, S. Nishimura, G. Suzaki, Y. Takanishi, K. Ishikawa, and H. Takezoe, Nat. Mater. **7**, 43 (2007).
4. J. Kobashi, H. Yoshida, and M. Ozaki, Nat. Photon. **10**, 389 (2016).
5. L. Wang, A. M. Urbas, and Q. Li, Adv. Mater. 1801335 (2018).
6. F. Zhai, Y. Feng, K. Zhou, L. Wang, Z. Zheng, and W. Feng, J. Materi. Chem. C **7**, 2146 (2019).
7. Y. Huang, Y. Zhou, C. Doyle, and S. T. Wu, Opt. Express **14**, 1236 (2006).

8. M. Mitov, Adv. Mater. **24**, 6260 (2012).
9. H. P. Yu, B. Y. Tang, J. H. Li, and L. Li, Opt. Express **13**, 7243 (2005).
10. L. Zhang, L. Wang, U. S. Hiremath, H. K. Bisoyi, G. G. Nair, C. V. Yelamaggad, A. M. Urbas, T. J. Bunning, and Q. Li, Adv. Mater. **29**, 1700676 (2017).
11. M. Xu, F. Xu, and D. K. Yang, J. Appl. Phys. **83**, 1938 (1998).
12. V. Sharma, M. Crne, J. O. Park, and M. Srinivasarao, Science **325**, 449 (2009).
13. W. J. Chung, J. W. Oh, K. Kwak, B. Y. Lee, J. Meyer, E. Wang, A. Hexemer, and S. W. Lee, Nature **478**, 364 (2011).
14. P. Chen, L. L. Ma, W. Hu, Z. X. Shen, H. K. Bisoyi, S. B. Wu, S. J. Ge, Q. Li, and Y. Q. Lu, Nat. Commun. **10**, 2518 (2019).
15. J. Xiang, A. Varanytsia, F. Minkowski, D. A. Paterson, J. M. Storey, C. T. Imrie, O. D. Lavrentovich, and P. Palffy-Muhoray, Proc. Natl. Acad. Sci. USA **113**, 12925 (2016).
16. Z. G. Zheng, B. W. Liu, L. Zhou, W. Wang, W. Hu, and D. Shen, J. Mater. Chem. C **3**, 2462 (2015).
17. L. J. Chen, Y. N. Li, J. Fan, H. K. Bisoyi, D. A. Weitz, and Q. Li, Adv. Opt. Mater. **2**, 845 (2014).
18. L. Wang, H. K. Bisoyi, Z. G. Zheng, K. G. Gutierrez-Cuevas, G. Singh, S. Kumar, T. J. Bunning, and Q. Li, Mater. Today **20**, 230 (2017).
19. J. Qin, X. Q. Wang, C. Yuan, Z. Zheng, and D. Shen, Liq. Cryst. **47**, 255 (2019).
20. K. G. Gutierrez-Cuevas, L. Wang, Z. G. Zheng, H. K. Bisoyi, G. Li, L. S. Tan, R. A. Vaia, and Q. Li, Angew. Chem. Int. Ed. Engl. **55**, 13090 (2016).
21. M. Wang, C. Zou, J. Sun, L. Zhang, L. Wang, J. Xiao, F. Li, P. Song, and H. Yang, Adv. Funct. Mater. **27**, 1702261 (2017).
22. T. H. Lin and H. C. Jau, Appl. Phys. Lett. **88**, 061122 (2006).
23. V. T. Tondiglia, L. V. Natarajan, C. A. Bailey, M. M. Duning, R. L. Sutherland, D. K. Yang, A. Voevodin, T. J. White, and T. J. Bunning, J. Appl. Phys. **110**, 053109 (2011).
24. R. B. Meyer, Appl. Phys. Lett. **12**, 281 (1968).
25. P. De Gennes, Solid State Commun. **6**, 163 (1968).
26. A. Matsuyama, Liq. Cryst. **45**, 153 (2017).
27. D. K. Yang and S. T. Wu, *Fundamentals of Liquid Crystal Devices,* 2nd Ed. (Wiley, 2014).
28. V. Borshch, Y. K. Kim, J. Xiang, M. Gao, A. Jakli, V. P. Panov, J. K. Vij, C. T. Imrie, M. G. Tamba, G. H. Mehl, and O. D. Lavrentovich, Nat. Commun. **4**, 2635 (2013).
29. G. Babakhanova, Z. Parsouzi, S. Paladugu, H. Wang, Y. A. Nastishin, S. V. Shiyanovskii, S. Sprunt, and O. D. Lavrentovich, Phys. Rev. E **96**, 062704 (2017).
30. J. Xiang, S. V. Shiyanovskii, C. T. Imrie, and O. D. Lavrentovich, Phys. Rev. Lett. **112**, 217801 (2014).
31. O. S. Iadlovska, G. R. Maxwell, G. Babakhanova, G. H. Mehl, C. Welch, S. V. Shiyanovskii, and O. D. Lavrentovich, Opt. Lett. **43**, 1850 (2018).
32. J. Xiang, Y. Li, Q. Li, D. A. Paterson, J. M. Storey, C. T. Imrie, and O. D. Lavrentovich, Adv. Mater. **27**, 3014 (2015).
33. M. Rumi, T. J. Bunning, and T. J. White, Soft Matter **14**, 8883 (2018).
34. S. M. Salili, J. Xiang, H. Wang, Q. Li, D. A. Paterson, J. M. Storey, C. T. Imrie, O. D. Lavrentovich, S. N. Sprunt, J. T. Gleeson, and A. Jakli, Phys. Rev. E **94**, 042705 (2016).
35. C. L. Yuan, W. Huang, Z. G. Zheng, B. Liu, H. K. Bisoyi, Y. Li, D. Shen, Y. Lu, and Q. Li, Sci. Adv. **5**, eaax9501 (2019).
36. J. J. Wu, Y. S. Wu, F. C. Chen, and S. H. Chen, Jpn. J. Appl. Phys. **41**, L1318 (2002).
37. J. S. Patel and R. B. Meyer, Phys. Rev. Lett. **58**, 1538 (1987).
38. D. Chen, J. H. Porada, J. B. Hooper, A. Klittnick, Y. Shen, M. R. Tuchband, E. Korblova, D. Bedrov, D. M. Walba, M. A. Glaser, J. E. Maclennan, and N. A. Clark, Proc. Natl. Acad. Sci. USA **110**, 15931 (2013).
39. H. K. Bisoyi and Q. Li, Chem. Rev. **116**, 15089 (2016).
40. H. K. Bisoyi and Q. Li, Angew. Chem. Int. Ed. Engl. **55**, 2994 (2016).
41. D. W. Berreman, J. Opt. Soc. Am. **62**, 502 (1972).
42. H. Wöhler, G. Haas, M. Fritsch, and D. Mlynski, J. Opt. Soc. Am. A **5**, 1554 (1988).